RSC Advances

PAPER

View Article Online
View Journal | View Issue

Cite this: *RSC Adv.*, 2021, **11**, 6509

Key parameters to enhance the antibacterial effect of graphene oxide in solution†

Grecia Guadalupe Montes-Duarte,[a] Guillermo Tostado-Blázquez,[a] K. L. S. Castro,[b] Joyce R. Araujo,[b] C. A. Achete,[b] José Luis Sánchez-Salas [a] and Jessica Campos-Delgado *[a]

Graphene oxide (GO) has lately become an interesting biomaterial due to its stunning properties and versatility, its claimed antimicrobial activity holds promise for potential health applications. Nonetheless, multiple reports investigating GO antibacterial activity lack rigor and uniformity on several aspects which are crucial when evaluating this effect. In this work, we highlight and address these parameters: morphology of the materials, exposure time, exposure methodology and concentration. We investigate the effect of GO and GO-based metallic composites observing these parameters on two pathogenic bacteria. Our nanomaterials have been characterized by means of SEM, EDX, DLS, FTIR and Raman spectroscopies. *Escherichia coli* and *Salmonella* Typhimurium suspended in saline solutions (no growth medium) have been exposed to GO (lateral size = 100 nm), silver nanoparticles, ceria nanoparticles, GO/silver and GO/ceria aqueous solutions for 0, 5, 15, 30, 60 and 90 minutes, before plating. Our experiments indicate that no prior exposure of the materials to bacteria (0 min) results in poor inactivation rates independently of concentration, while increasing times of interaction enhance inactivation. Moreover, our experiments show concentration-dependent results showing higher activity for concentrations of 100 μg mL^{-1}; and prove that 30 minutes of exposure are sufficient to deploy the antimicrobial effects of these materials. GO possesses the lowest inactivation rate, and the presence of silver and ceria nanoparticles in the GO surface boosts its antimicrobial effect. Thus, the enhancement of the antibacterial activity of graphene oxide relies on 30 minutes of interaction in water, concentration of 100 μg mL^{-1}, and its decoration by silver/ceria nanoparticles.

Received 17th September 2020
Accepted 14th January 2021

DOI: 10.1039/d0ra07945f

rsc.li/rsc-advances

1. Introduction

Water decontamination is a major concern in places where the availability of drinking water is scarce; in particular, the inactivation of pathogenic bacteria present in water is vital to avoid bacterial gastroenteritis. A wide spectrum of alternatives for this goal are attainable based on different technologies. One of these alternatives is nanotechnology, where, metallic and non-metallic nanomaterial options have been explored, presenting different mechanisms responsible for their antibacterial activity. Graphene oxide (GO), is a 2D carbon nanomaterial that combines the availability of honey-comb basal planes decorated with oxygen-based functional groups, which render it hydrophilic. Some studies have reported the cytotoxic effect of graphene oxide,[1–4] while others focus on its antibacterial response.[5–14] In the last ten years, many studies have been performed in order to document its antibacterial effect without a clear consensus. These controversial results can be explained by the different experimental conditions used in each report: the different sizes of the graphene oxide samples, the exposure time and medium (water, saline solution, phosphate-buffered saline solution, growth medium), and the different growth conditions (plating, growth in suspension, over a membrane). Its antibacterial activity has been attributed to different mechanisms: membrane piercing by the edges of GO, oxidative stress by the production of ROS and/or electron transfer, bacteria wrapping by large GO sheets and trapping over membranes.[15] A very complete and critical review on the effect of GO on bacteria in suspension has been carried out by V. Palmieri and co-authors.[15] This review summarizes the articles that have reported enhancement effect, no effect, and inhibition effect; as well as those that report size-dependence, interaction conditions-dependence, and concentration-dependence.

Something undeniable is that a lot of parameters are involved in the experiments and play a crucial role in the results reported, such as: purity of GO; size and morphology of GO; and their interaction conditions (incubation time, concentration,

[a]*Universidad de las Américas Puebla, Departamento de Ciencias Químico Biológicas, ExHacienda Sta. Catarina Mártir S/N, San Andrés Cholula, Puebla, 72810, Mexico. E-mail: jessica.campos@udlap.mx*

[b]*Instituto Nacional de Metrologia, Qualidade e Tecnologia, Av. Nossa Sra. das Graças, 50, 25250-020 Duque de Caxias, Brazil*

† Electronic supplementary information (ESI) available. See DOI: 10.1039/d0ra07945f

exposure methodology, *etc.*).[7–15] A good example of this is the work by Barbolina and co-authors,[9] who explored the influence of the purity of GO samples on their effect of *E. coli* and *S. aureus*. The authors demonstrated that a highly pure GO sample has no adverse effect on bacteria; they explored different incubation times, concentrations (up to 1 mg mL^{-1}) and GO sizes, reporting no difference between large and small flakes, claiming that the only adverse effect was the residual contamination of the synthesis process. However, the exposure of bacteria to GO was carried out in the presence of growth medium, which has proven to saturate the basal planes of graphene and suppress any effect it could have.[7] In a previous contribution by our group,[10] we performed a systematic study of the antibacterial effect of GO on *E. coli* by monitoring the dynamic growth measuring the OD (optical density) of bacterial suspensions; the interaction of the material with bacteria was carried out in saline solution for 1 h, observing concentration- and size-dependent effects, agreeing with the results of other reports under the same experimental conditions.[8,12,13]

Silver has been known to possess antibacterial effects,[16] this property has also been confirmed for its nanostructured counterpart.[17] The effect of composite materials containing GO and silver nanoparticles has also been studied against Gram-negative and Gram-positive bacteria.[18–25] Jacovone and co-authors,[26] report the antibacterial effect of GO/Ag composites and GO against *E. coli*; their results show that GO tested alone showed no adverse effects while the composite material showed inactivation at concentrations of 100 μg mL^{-1}. It is worth highlighting the fact that the exposure was carried out in phosphate buffer solution. Ceria nanoparticles have also been studied synergistically with GO; Kashinath and co-authors[27] report the effect of this composite material against *S. aureus* and *P. aeruginosa*, demonstrating high inactivation rates.

In this study we monitored the effect of concentration, exposure times and exposure in the absence of growth medium (in sterile water) of GO, Ag nanoparticles, ceria nanoparticles and GO-based composites (GO/Ag and GO/CeO_2) against *Escherichia coli* and *Salmonella enterica* serovar Typhimurium by colony forming units (CFU) enumeration. Our findings reveal that relative short exposure times (30 minutes) are needed to deploy the antimicrobial activity of the materials, span times of hours did not necessarily potentiated the effects. Concentration-dependent effects were found for GO and the composites; moreover, our findings evidenced that from all the materials tested, GO was the less effective and that silver and ceria in the composite materials boosted the GO antibacterial response.

2. Methodology

2.1 Materials synthesis

$AgNO_3$, $NaBH_4$, $Ce(NO_3)_3 \cdot 6H_2O$ and $C_6H_{12}N_4$ were purchased from Sigma-Aldrich and were used without any further purification. In all procedures, ultrapure sterile water HPLC quality was used, all laboratory materials were sterilized prior to be used.

GO. Graphene oxide was exfoliated from graphite oxide (GtO) by ultrasonication. Graphite oxide was prepared according to the Hummers' method as described elsewhere.[28] Solutions of GtO in water at concentrations of 1 mg mL^{-1} were placed in glass containers and subjected to ultrasonic bath (Cole-Parmer) for 6 hours. After this time, the homogeneous solutions were centrifuged for 30 minutes at 6000 rpm in order to precipitate the few-layer graphene, the supernatant containing monolayered GO was recovered and the precipitate weighed to determine the final solution concentration.

Silver nanoparticles (Ag). The metallic particles were synthesized by chemical reduction,[29] adding 20 mL of 1.0 mM $AgNO_3$ dropwise to 60 mL of 2 mM $NaBH_4$ in an ice bath with magnetic stirring. Since the addition of 3 mL of $AgNO_3$, the characteristic yellow color was appreciated. As higher amounts of the precursor were added, the color of the solution became more intense. Once the addition was complete, stirring was stopped.

Cerium oxide nanoparticles (CeO_2, ceria). The synthesis of ceria nanoparticles was based on the report by Zhang, Jin & Chan.[30] 50 mL of 1 M stock solutions of $Ce(NO_3)_3 \cdot 6H_2O$ and $C_6H_{12}N_4$ were prepared. Subsequently, both solutions were diluted to obtain 400 mL of 37.5 mM $Ce(NO_3)_3 \cdot 6H_2O$ and 30 mL of 0.5 M $C_6H_{12}N_4$; then, they were mixed and magnetically stirred at low speed for 24 hours. Finally, the solution was centrifuged at 12 000 rpm at 25 °C for 30 minutes to remove any precipitate.

Composites. Two methodologies were followed to prepare GO/Ag composites, labelled GO/Ag1 and GO/Ag2, one composite material of ceria and GO was prepared, GO/CeO_2.

GO/Ag1. The methodology consisted of adding 15 mL of Ag nanoparticles and 7.5 mL of GO to a conical centrifuge tube with 7.5 mL of water. This solution was stirred using a Vortex mixer for 15 minutes.

GO/Ag2. The composite was prepared according to the methodology proposed by Kamali, with minor modifications.[31] Briefly, 2.925 mL of GO, 12.07 mL of water and 5 mL of an 85% w/v solution of $AgNO_3$ were mixed using a tip Ultrasonic Processor Vibra Cell (model VC130PB, 120 V, 50/60 Hz, USA) at 50 W for 15 minutes. The solution was placed in an ice bath during this process to avoid vibration-induced heating. Finally, 200 mL of 5 mM $NaBH_4$ were gradually added without stirring, turning the solution yellowish. Subsequently, 15 mL of water were added. The solution had a mustard yellow color at the end of the synthesis, the next day its shade was grayish.

GO/CeO_2. 15 mL of CeO_2 nanoparticles, 7.5 mL of GO and 7.5 mL of water were mixed in a sterile conical centrifuge tube. This solution was stirred using a Vortex mixer for 15 minutes.

2.2 Characterization

SEM. Scanning electron microscopy was carried out using a Maia 3 Tescan instrument coupled with a Bruker Quantax XFlash® 6|100 X-ray detector to perform energy-dispersive X-ray spectroscopy (EDX). Samples in water suspensions were prepared on aluminum pins using double-sided carbon tape.

For each sample, a drop of the solution was placed on the carbon tape and the solvent was allowed to dry in air.

Raman spectroscopy. Raman spectroscopy was performed using a Horiba XploRa microRaman spectrometer in the back-scattering configuration coupled with a 532 nm wavelength laser; measurements were recorded using a 600 gr mm^{-1} diffraction grating and a 100× objective. In order to guarantee measurements without interference of the substrate, silicon was chosen since it presents a sharp reflection at ~521 cm^{-1} and minor features at low frequencies. For sample preparation, a drop of each suspension was placed on a silicon substrate and allowed to dry on a hot plate at ~80 °C.

Fourier-transform infrared spectroscopy. Fourier-transform infrared spectroscopy was carried out using an Agilent Cary-630 instrument, equipped with a diamond ATR detector with a 1 mm diameter sampling surface; all the dried samples were analyzed at a spectral resolution of 8 cm^{-1}, over a wavenumber range of 4000–500 cm^{-1}. For each sample one drop of the suspension was placed in the sample position, letting it dry under light irradiation, this procedure was repeated 3–4 times. After each measurement, the equipment was fully cleaned with ethanol and the spectra of ethanol was acquired to make sure that no residues of the previous material were left. The data was plotted as recorded, no treatment was done to the spectra.

2.3 Biological tests

The bacterial inactivation properties of the materials were evaluated using a fresh culture of *Escherichia coli* ATCC 25923 and *Salmonella enterica* serovar Typhimurium, both strains were obtained from the strain collection of the Microbiology Research Laboratory at Universidad de las Americas Puebla. Each strain was cultured in Petri dishes containing MacConkey agar (Bioxon®) and incubated overnight at 37 °C. The culture was suspended in saline isotonic sterile solution (SISS) (NaCl 0.85%) and its cell concentration was adjusted to the turbidity of tube no. 2 of the McFarland standard, which corresponds to ~6×10^8 colony forming units per mL (CFU mL^{-1}).[32]

10 mL solutions in sterile water of each material were prepared at different concentrations (1, 10 and 100 μg mL^{-1}; for controls, sterile saline solution was used). For Ag nanoparticles only concentrations of 1 and 10 μg mL^{-1} were tested. Then, 100 μL of the bacterial suspension to be evaluated (*E. coli* or *Salmonella* Typhimurium) were added to each solution to obtain an initial bacterial concentration of ~10^6 CFU mL^{-1}. When the material came into contact with the microorganism, counting of the exposure time began and each solution was divided into 6 vials; each corresponding to a given time (0, 5, 15, 30, 60 and 90 min), the vials were shaken at 170 rpm at 37 °C for the stipulated time. Once each exposure time was completed, a 100 μL aliquot was taken from the corresponding vial and added to 900 μL of sterile water. Subsequently, each solution was serially diluted four more times maintaining the same ratio (1 : 10) using sterile water. Finally, 10 μL were taken from each dilution and plated in duplicate in Petri dishes with Muller–Hinton agar (Bioxon®) previously gridded. All plates were allowed to stand overnight at room temperature (25 °C) to permit a slow growing and avoid colonies overgrow. The next morning, the plates were incubated at 37 °C for two hours and then the colony count was carried out. The procedure was performed in duplicate for each experiment on different days.

3. Results and discussion

3.1 Characterization

In order to investigate the morphology of our samples, scanning electron microscopy studies were performed. Fig. 1 presents representative images of the starting materials and their composites. As detailed in the Methods section, samples were drop-coated on top of carbon tape. Fig. 1a shows a representative image of GO; since the undiluted suspension of GO was used, the result is a GO film once the water evaporated, isolated GO flakes are not visible due to the high concentration of the used solution. The GO film is quite transparent and our observations revealed a homogeneous material without traces of contamination, EDX analysis (ESI, Fig. S1†) confirmed signals exclusively of C and O. Silver nanoparticles are very small, they are visible as bright dots in Fig. 1b, due to the small size of the nanomaterials, it was not possible to collect signal from Ag in the EDX analysis. The semiconductive nature of CeO_2, made imaging of ceria nanoparticles difficult, a low-resolution image can be found in Fig. 1c, the material consists of aggregated spherical nanoparticles, which can be better appreciated in STEM mode (Fig. S2a, ESI†). The nature of the nanomaterial was confirmed by EDX, where signals corresponding to cerium and oxygen appear, along with signal from nitrogen that is derived from the use of cerium nitrate and hexamine during synthesis (Fig. S2b, ESI†).

For composite GO/Ag1, the morphology of the sample is similar to GO, a continuous film of GO is visible once water is evaporated, bright dots appear randomly and scarcely within the film, corresponding to individual spherical Ag nanoparticles. Composite GO/Ag2 shows a different morphology, the flakes of GO are visible, accompanied by isolated Ag spherical nanoparticles spread within the sheets. The morphological differences of both composites containing Ag lie in the synthesis methodologies of each one. In the case of the composite GO/Ag1, a larger amount of GO was used compared to GO/Ag2, which is reflected in its morphology, showing a continuous film of this material instead of flakes as in the case of the composite GO/Ag2. Regarding the Ag nanoparticles present in the materials, a larger amount of silver precursor ($AgNO_3$) was used during synthesis of the second composite, consequently, composite GO/Ag2 shows a greater amount and a better distribution of the metallic nanoparticles; unlike the composite GO/Ag1, where the presence of these particles was limited, indicating a low concentration of Ag, which would explain the difficulty in detecting this element in subsequent measurements for this composite (EDX, FTIR and Raman spectroscopy). Composite GO/CeO_2 shows a very interesting morphology, constituted of interconnected graphene sheets supporting ceria nanoparticles.

Further information on the size of the materials was obtained by dynamic light scattering (DLS), Ag and CeO_2

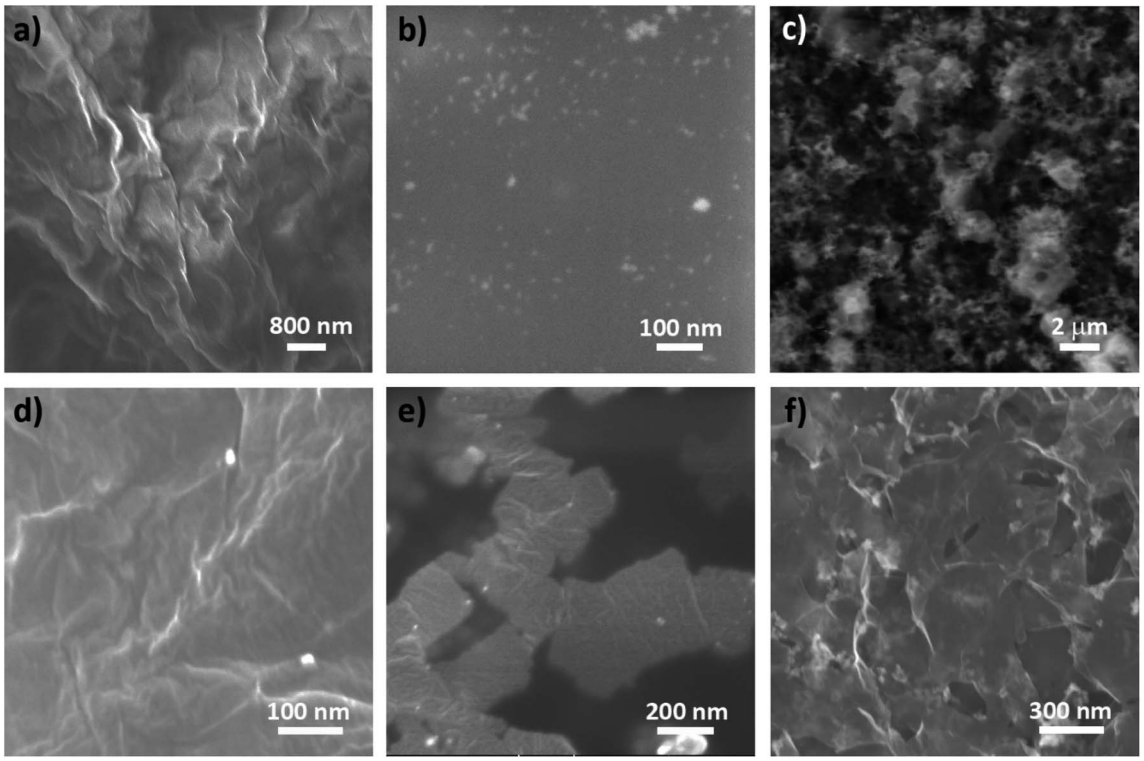

Fig. 1 Scanning electron micrographs of the studied materials reveal their morphology, (a) graphene oxide, clean graphene oxide sheets form a uniform membrane as the solvent evaporates from the concentrated solution; (b) silver nanoparticles, spherical nanoparticles well dispersed can be seen; (c) ceria nanoparticles, aggregated nanoparticles along with residues of the synthesis precursors can be evidenced; (d) GO/Ag1, (e) GO/Ag2, and (f) GO/CeO_2; all composites show the GO flakes along with nanoparticles although each presents different morphology. Samples have been prepared by drop-coating on top of double-sided carbon tape.

nanoparticles were studied because of their spherical morphologies. For Ag nanoparticles, most of the material showed a hydrodynamic diameter of 38.2 nm, 70% of the total volume, while the rest exhibited a hydrodynamic diameter of 1.37 nm (Fig. S3a†). CeO_2 nanoparticles also showed two diameter distributions (Fig. S3b†), the most abundant (∼74%) at 376 nm, and a small proportion at 1363 nm (∼26%), surely corresponding to large aggregates of clustered nanoparticles as can be observed in Fig. 1c and S2a.†

Our samples have been investigated using Raman spectroscopy, Fig. 2a and b show representative spectra of the samples, signals have been normalized to the main reflection of silicon at ∼521 cm^{-1}, all measurements show the typical silicon bands, identified by the symbol *. The GO spectrum presents the features that can be attributed to the D and the G bands, at ∼1350 and ∼1580, cm^{-1}, respectively. The presence of the G band confirms the graphitic nature of the material and the D band arises as defects are encountered in the honey-comb network, the functional groups present in graphene oxide are responsible for the high intensity of this reflection. In Fig. 2a the response of Ag nanoparticles is plotted, where the characteristic reflection of Ag–O can be found.[33] Composite material GO/Ag1 only shows the D and G bands, confirming the presence of GO in the material, however, no signal from silver could be detected in our measurements, which points to the scarce quantity of silver in the composite. Material GO/Ag2 also shows the D and G bands; moreover, the silver-related feature is also present, confirming the presence of GO and Ag nanoparticles.

Raman measurements of ceria nanoparticles reveal the presence of the crystalline phase of CeO_2 by the appearance of a feature at ∼450 cm^{-1} (identified by # in Fig. 2b),[34] however other high intensity features denote the presence of more compounds. A reflection at ∼800 cm^{-1} (identified by +) proves the presence of hexamine residues[35] and at higher frequency at ∼1040 cm^{-1} we find the typical reflection of nitrates (identified by °), which can be related to cerium nitrate used as synthesis precursor.[36] The identification of these bands, demonstrates that the precursors were not fully consumed during the production of ceria nanoparticles. The signal corresponding to GO/CeO_2 shows very intense D and G bands, confirming the presence of GO; low intensity features in the positions corresponding to bands related to the precursors and CeO_2 can also be identified.

FTIR spectroscopy of GO and Ag composites, see Fig. 2c, show strong reflections related to water, signaled by black arrows. The U-shaped characteristic peak of the –O–H stretch mode at ∼3300 cm^{-1}, along with the peak at ∼1635 cm^{-1}, attributed to the –OH bend mode.[37] However, the procedure described for the measurements guaranteed that the measurements were not carried out on liquid state, pointing to water absorption being responsible for the resulting spectra, demonstrating the high hydrophilicity of the materials. These

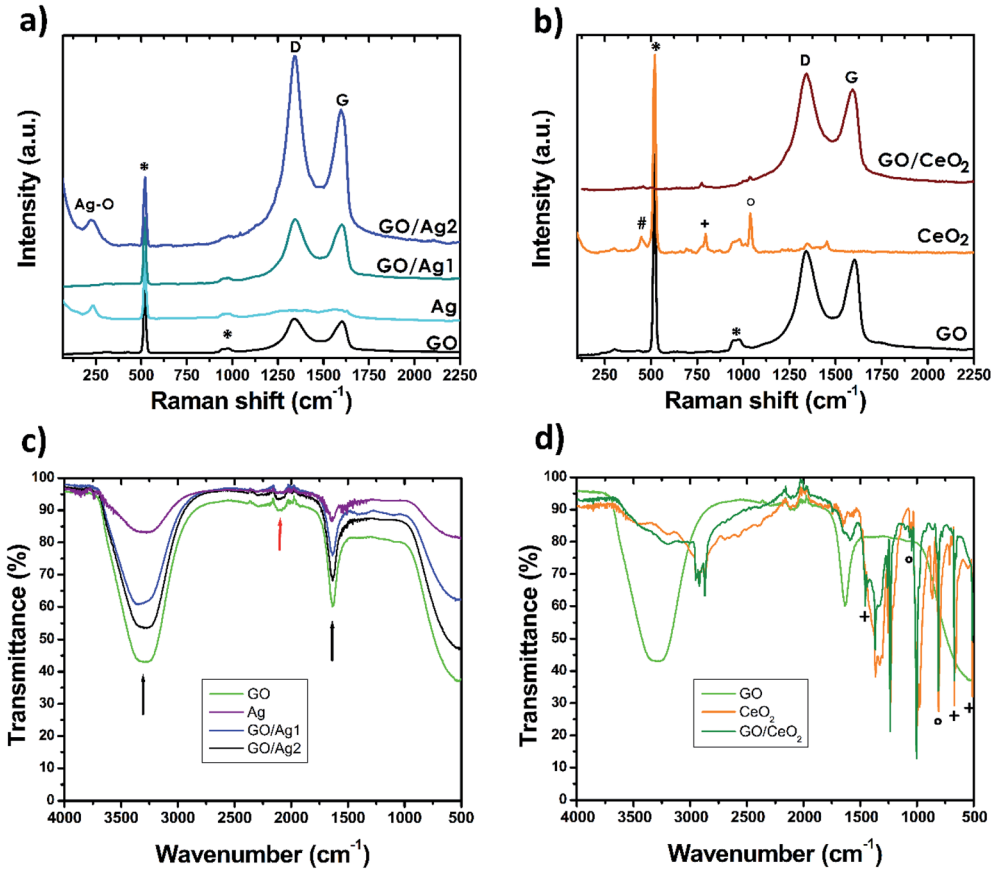

Fig. 2 Raman and FTIR spectroscopy analysis of the samples. Characteristic Raman spectra of (a) GO and Ag-related materials and (b) GO and CeO_2-related materials. Composites show reflections of sp^2 hybridized carbon (G-band) attributed to GO as well as bands that confirm the presence of nano silver and nano ceria in (a) and (b), respectively. Features identified by * are silicon-related reflections. FTIR analysis of the (c) silver and (d) ceria composites. Water- and CO_2-related features are signaled by black and red arrows, respectively. The strong water-related bands confirm the hydrophilic nature of our materials. Features identified by #, + and ° correspond to signals from CeO_2, hexamine and cerium nitrate, respectively.

bands are also present, although with less intensity, on the signal from CeO_2 and GO/CeO_2, see Fig. 2d. The FTIR spectrum of CeO_2 and GO/CeO_2 demonstrate reflections coming from hexamine residues at ~510, 670 and 1456 cm^{-1} that are related to ring deformation, N–C–N bending, and CH_2 scissors, respectively (denoted by + in Fig. 2d).[38]. Other absorption peaks found at ~810, 1046 and 1058 cm^{-1} can be attributed to cerium nitrate (denoted by °, in Fig. 2d),[36] confirming the results of Raman spectroscopy for the same materials.

All samples showed weak bands in the region between 1900 and 2300 cm^{-1} (red arrow in Fig. 2c) attributed to the asymmetric vibrational modes of CO_2 absorbed in the sample from the atmosphere.

3.2 Antibacterial effects

As described in the introduction, several factors are crucial when testing the antibacterial effect of GO, among them: purity, size of the flakes, time and way of exposure and concentration. All of these parameters influence the result of biocompatibility tests. In this study, our characterization and previous works account for the purity of GO;[10,23] the flakes used show lateral dimensions of 100 nm according to previous reports.[10] Regarding the exposure methodology, we have chosen to carry out the first contact of our materials with bacteria in water, to eliminate the effect of medium components that could block the antibacterial activity.[7] Six exposure times have been investigated: 0, 5, 15, 30, 60 and 90 minutes. Finally, three concentrations were used: 1, 10 and 100 μg mL^{-1}, a diagram of the procedure can be found in Fig. 3.

Fig. S4 and S5† contain results for the CFU enumeration for *Escherichia coli* and *Salmonella* Typhimurium, respectively and can be found in the ESI file.† These figures contain 6 graphs each, plotting time of exposure *vs.* CFUs, each graph includes the results for the three concentrations tested. Results evidence that no previous interaction of the materials with bacteria (0 minutes exposure time, independently of the concentration used) allows bacteria survival, while systematically increasing the exposure times leads to increasing inactivation rates (lower CFU counts).

All materials tested in this work showed antibacterial activity against both Gram negative bacteria (*E. coli* and *Salmonella* serovar Typhimurium). However, *S.* Typhimurium was slightly more sensitive than *E. coli*.

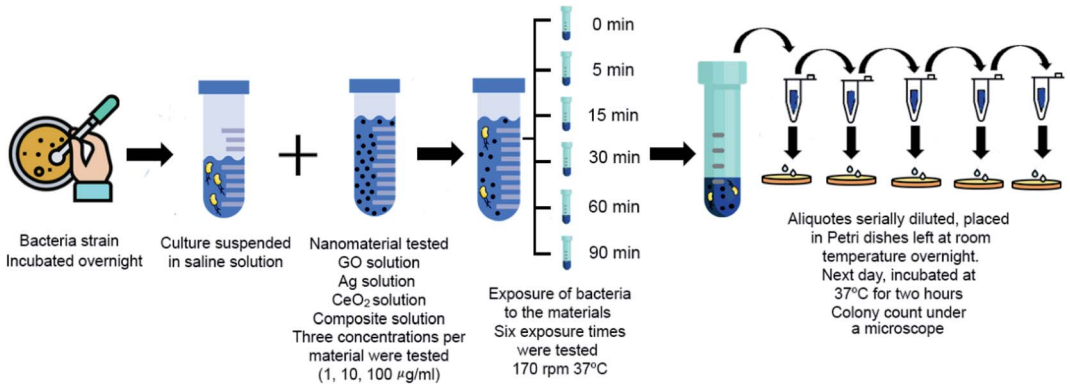

Fig. 3 Schematic representation of the procedure carried out for the biological tests. Prior contact of the tested nanomaterials with the microorganism in the absence of growth medium and the time allowed for interaction (0, 15, 30, 60 and 90 minutes) are key parameters in this study.

GO, even at the highest concentration tested (100 μg mL^{-1}), was the less effective material against both bacteria. However, GO achieved higher inactivation rates for *S.* Typhimurium, this tendency was also observed for Ag since *S.* Typhimurium was more sensitive to silver than *E. coli*. The sensitivity difference could be due to the external structure because even though both bacteria are Gram negative, different sugars are found in their lipopolysaccharides.[39] Other plausible reason is due to the enzymes in charge of eliminating reactive oxygen species (ROS) as catalase or the sensitivity of some vital structures to these ROS for each bacteria.[40]

The best material that could inactivate both bacteria was Ag, silver nanoparticles, and both concentrations tested, 1 and 10 μg mL^{-1}, drove quite similar effects. This result did not come as a surprise since silver is known as an effective antimicrobial[16,17,40] and this case was not the exception. An interesting finding was the effect of GO when combined with silver for composites GO/Ag1 and GO/Ag2. Silver was found to increase the GO antibacterial activity, needing shorter exposure times and being able to achieve full inactivation. The same effect was observed for CeO_2 with GO (GO/CeO_2) although not as dramatic as the silver case, higher inactivation rates were measured when GO was coupled with CeO_2, see bottom graphs of Fig. S4 and S5.†

For comparison sake, the average CFU values were normalized dividing the number of counts for each exposure time (N) by the number of counts at time of exposure zero (N_0). The concentrations showing the highest inactivation rates (lowest N/N_0 values) for each material were selected for both bacteria, Fig. 4 contains plots of these results as a function of exposure time.

Fig. 4a shows that for *E. coli*, the highest concentrations tested for each material showed the best inactivation rates; however, the only material that did not fully inactivate this strain was GO, the same effect was observed for *S.* Typhimurium but inactivation was mildly higher, see Fig. 4b. As highlighted above, the combination of Ag and CeO_2 with GO improved its antimicrobial effects, achieving full inactivation at short exposure times. Observing this graph, we can generalize that the full potential of inactivation for the materials tested can be achieved after 30 minutes of exposure in saline solution, it is worth pointing out that, if exposure were carried out in the presence of culture broth or media, results could be completely different, as reported by Hui and co-authors.[7]

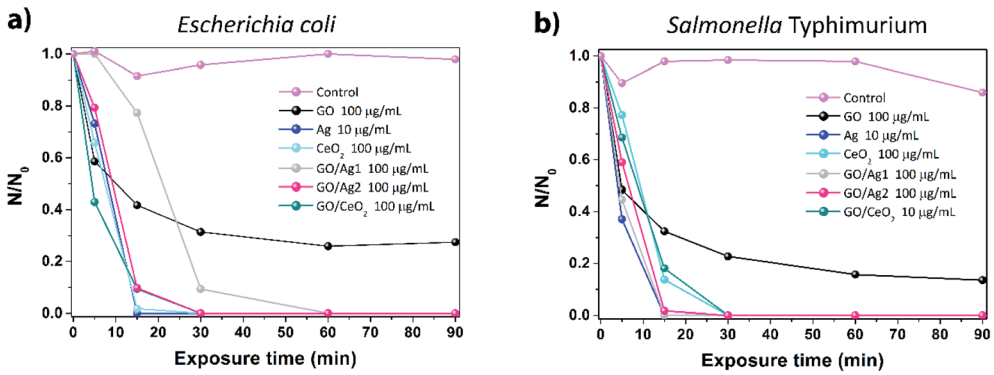

Fig. 4 Concentrations showing the highest inactivation rates for each material tested for Gram negative bacteria (a) *Escherichia coli* and (b) *Salmonella enterica* Typhimurium. GO was the least effective material; as general trend, the highest concentrations showed best inactivation rates and 30 minutes of exposure time are sufficient to deploy the material's activity.

4. Conclusions

GO, silver nanoparticles, ceria nanoparticles and composites of these materials have been studied and tested for inactivation of *Escherichia coli* and *Salmonella* Typhimurium. The exposure to bacteria was carried out in sterile water at 0, 5, 15, 30, 60 and 90 minutes and three concentrations have been tested (1, 10 and 100 μg mL^{-1}). Results evidence that no previous interaction of the materials with bacteria (0 minutes exposure time) allows cells viability, while systematically increasing the exposure times leads to increasing inactivation rates. Most materials achieve their full inactivation potential at exposure times of 30 minutes. As a general trend, higher concentrations were more effective for inactivation. GO showed to be less toxic than all the tested materials, for the bacteria tested in this work, showing a concentration-dependent effect. Our experiments show that the only material that could not fully inactivate the tested bacteria was GO, demonstrating lower toxicity than silver and ceria nanoparticles. Moreover, silver and ceria nanoparticles coupled with GO, boosted its activity, demonstrating higher inactivation rates and needing shorter exposure times to achieve full inactivation. Our results highlight key parameters to increase the antibacterial activity of GO: exposure methodology (prior interaction in water), exposure time (30 minutes), concentration (100 μg mL^{-1}) and the introduction of metallic nanoparticles decorating the sheets. This study proposes materials based on GO having the potential to develop water systems to eliminate Gram-negative bacteria (coliforms) that can produce water borne diseases (*i.e.* typhoid fever) and therefore reduce gastroenteritis in places where safe drinking water is not available. We envisage the realization of a systematic study focusing on the defined key parameters considering pathogenic Gram-positive bacteria, in order to compare the effect of GO-based materials on different shaped microorganisms.

Conflicts of interest

There are no conflicts of interest to declare.

Acknowledgements

J. C.-D. is thankful to A. R. Ruiz-Hernández, J. F. Vega-Clemente, A. Gutierrez-Cruz and O. Betanzos-Sanchez for technical assistance. J. C.-D. thanks UDLAP for funding.

References

1 L. Q. Chen, P. P. Hu, L. Zhang, S. Z. Huang, L. F. Luo and C. Z. Huang, *Sci. China: Chem.*, 2012, **9**(2), 1343–1351.
2 A. Sasidharan, L. S. Panchakarla, P. Chandran, D. Menon, S. Nair, C. N. R. Rao and M. Koyakutty, *Nanoscale*, 2011, **3**(6), 2461–2464.
3 Y. Chang, S. T. Yang, J. H. Liu, E. Dong, Y. Wang, A. Cao, Y. Liu and H. Wang, *Toxicol. Lett.*, 2011, **200**(3), 201–210.
4 S. A. Sydlik, S. Jhunjhunwala, M. J. Webber, D. G. Anderson and R. Langer, *ACS Nano*, 2015, **9**(4), 3866–3874.
5 O. Akhavan and E. Ghaderi, Toxicity of graphene and graphene oxide nanowalls against bacteria, *ACS Nano*, 2010, **4**(10), 5731–5736.
6 S. Liu, T. H. Zeng, M. Hofmann, E. Burcombe, J. Wei, R. Jiang, J. Kong and Y. Chen, Antibacterial activity of graphite, graphite oxide, graphene oxide and reduced graphene oxide: membrane and oxidative stress, *ACS Nano*, 2011, **5**(9), 6971–6980.
7 L. Hui, J.-G. Piao, J. Auletta, K. Hu, Y. Zhu, T. Meyer, H. Liu and L. Yang, Availability of the basal planes of graphene oxide determines whether it is antibacterial, *ACS Appl. Mater. Interfaces*, 2014, **6**, 13183–13190.
8 F. Perreault, A. Fonseca de Faria, S. Nejati and M. Elimelech, Antimicrobial properties of Graphene oxide nanosheets: why size matters, *ACS Nano*, 2015, **9**(7), 7226–7236.
9 I. Barbolina, C. R. Woods, N. Lozano, K. Kostarelos and I. S. Roberts, Purity of graphene oxide determines its antibacterial activity, *2D Mater.*, 2016, **3**, 025025.
10 J. Campos-Delgado, K. L. S. Castro, J. G. Munguia-Lopez, A. K. Gónzalez, M. E. Mendoza, B. Fragneaud, R. Verdan, J. R. Araujo, F. J. González, H. Navarro-Contreras, I. N. Pérez-Maldonado, A. de León-Rodríguez and C. A. Achete, Effect of graphene oxide on bacteria and peripheral blood mononuclear cells, *J. Appl. Biomater. Funct. Mater.*, 2016, **14**(4), e423–e430.
11 F. Zou, H. Zhou, D. Y. Jeong, J. Kwon, S. U. Eom, T. J. Park, S. W. Hong and J. Lee, Wrinkled surface-mediated antibacterial activity of graphene oxide nanosheets, *ACS Appl. Mater. Interfaces*, 2017, **9**, 1343–1351.
12 S. Liu, M. Hu, T. H. Zeng, R. Wu, R. Jiang, J. Wei, L. Wang, J. Kong and Y. Chen, Lateral dimension-dependent antibacterial activity of graphene oxide sheets, *Langmuir*, 2012, **28**(33), 12364–12372.
13 V. Palmieri, F. Bubli, M. C. Lauriola, M. Caci, R. Torelli, G. Ciasca, C. Conti, M. Sanguinetti, M. Papi and M. De Spirito, Bacteria meet graphene: modulation of graphene oxide nanosheets interaction with human pathogens for an effective antimicrobial therapy, *ACS Biomater. Sci. Eng.*, 2017, **3**(4), 619–627.
14 C.-H. Yu, G.-Y. Chen, M.-Y. Xia, Y. Xie, Y.-Q. Chi, Z. Y. He, C.-L. Zhang, T. Zhang, Q.-M. Chen and Q. Peng, Understanding the sheet size-antibacterial activity relationship of graphene oxide and the nano-bio interaction-based physical mechanisms, *Colloids Surf., B*, 2020, **191**, 111009.
15 V. Palmieri, M. C. Lauriola, G. Ciasca, C. Conti, M. De Spirito and M. Papi, The Graphene oxide contradictory effects against human pathogens, *Nanotechnology*, 2017, **28**, 152001.
16 K. Mijnendonckx, N. Leys, J. Mahillon, *et al.*, Antimicrobial silver: uses, toxicity and potential for resistance, *BioMetals*, 2013, **26**, 609–621.
17 C. Marambio-Jones and E. M. V. Hoek, A review of the antibacterial effects of silver nanomaterials and potential implications for human health and the environment, *J. Nanopart. Res.*, 2010, **12**, 1531–1551.

18 J. Tang, Q. Chen, L. Xu, S. Zhang, L. Feng, L. Cheng, H. Xu, Z. Liu and R. Peng, Graphene Oxide−Silver Nanocomposite As a Highly Effective Antibacterial Agent with Species-Specific Mechanisms, *ACS Appl. Mater. Interfaces*, 2013, **5**(9), 3867–3874.

19 J. D. Kim, H. Yun, G. C. Kim, C. W. Lee and H. C. Choi, Antibacterial activity and reusability of CNT-Ag and GO-Ag nanocomposites, *Appl. Surf. Sci.*, 2013, **283**, 227–233.

20 A. A. Menazea and M. K. Ahmed, Synthesis and antibacterial activity of graphene oxide decorated by silver and copper oxide nanoparticles, *J. Mol. Struct.*, 2020, **1218**, 128536.

21 A. F. de Faria, A. C. M. de Moraes, P. D. Marcato, D. S. T. Martinez, N. Duran, A. G. Souza Filho, A. Brandelli and O. L. Alves, Eco-friendly decoration of graphene oxide with biogenic silver nanoparticles: antibacterial and antibiofilm activity, *J. Nanopart. Res.*, 2014, **16**, 2110.

22 L. T. Tam, N. X. Dinh, N. V. Cuong, N. V. Quy, T. Q. Huy, D.-T. Ngo, K. Mølhave and A.-T. Lej, Graphene Oxide/Silver Nanohybrid as Multi-functional Material for Highly Efficient Bacterial Disinfection and Detection of Organic Dye, *J. Electron. Mater.*, 2016, **45**(10), 5321–5333.

23 S. Jaworski, *et al.*, Graphene Oxide-Based Nanocomposites Decorated with Silver Nanoparticles as an Antibacterial Agent, *Nanoscale Res. Lett.*, 2018, **13**, 116.

24 C. Angulo-Pineda, P. Palma, J. Bejarano, A. Riveros, M. Kogan and H. Palza, Antibacterial Silver Nanoparticles Supported on Graphene Oxide with Reduced Cytotoxicity, *JOM*, 2019, **71**(10), 3698–3705.

25 R. Thomas, J. Unnikrishnan, A. V. Nair, E. C. Daniel and M. Balachandran, Antibacterial performance of GO–Ag nanocomposite prepared via ecologically safe protocols, *Appl. Nanosci.*, 2020, **10**, 4207–4219.

26 R. M. S. Jacovone, J. J. S. Soares, T. S. Sousa, *et al.*, Antibacterial activity of silver/reduced graphene oxide nanocomposite synthesized by sustainable process, *Energy Ecol. Environ.*, 2019, **4**, 318–324.

27 L. Kashinath, K. Namratha and K. Byrappa, Microwave mediated synthesis and characterization of CeO2-GO hybrid composite for removal of chromium ions and its antibacterial efficiency, *J. Environ. Sci*, 2019, **76**, 65–79.

28 K. L. S. Castro, R. V. Curti, J. R. Araujo, S. M. Landi, E. H. M. Ferreira, R. S. Neves, A. Kuznetsov, L. A. Sena, B. S. Archanjo and C. A. Achete, Calcium incorporation in graphene oxide particles: a morphological, chemical, electrical and thermal study, *Thin Solid Films*, 2016, **610**, 10–18.

29 L. Mulfinger, S. D. Solomon, M. Bahadory, A. V. Jeyarajasingam, S. A. Rutkowsky and C. Boritz, Synthesis and Study of Silver Nanoparticles, *J. Chem. Educ.*, 2007, **84**(2), 322.

30 F. Zhang, Q. Jin and S.-W. Chan, Ceria nanoparticles: size, size distribution, and shape, *J. Appl. Phys.*, 2004, 4319–4326.

31 K. Z. Kamali, A. Pandikumar, G. Sivaraman, H. N. Lim, S. P. Wren, T. Sun and N. M. Huan, Silver@graphene oxide nanocomposite-based optical sensor platform for biomolecules, *RSC Adv.*, 2015, 17809–17816.

32 Dalynn Biologicals, *McFarland Standard*, 2002, retrieved from http://www.dalynn.com/dyn/ck_assets/files/tech/TM53.pdf.

33 J.-C. Valmalette, Z. Tan, H. Abe and S. Ohara, Raman scattering of linear chains of strongly coupled Ag nanoparticles on SWCNTs, *Sci. Rep.*, 2014, **4**, 5238.

34 R. Kostic, S. Askrabic, Z. Dohcevic-Mitrovic and Z. V. Popovic, Low-frequency Raman scattering from CeO_2 nanoparticles, *Appl. Phys. A: Mater. Sci. Process.*, 2008, **90**, 679–683.

35 R. Tong, X. Hu, G. Fang, S. Sun, J. Liu and S. Wang, Rapid detection of hexamethylentetramine based on the substrate UC@SiO2@Au@Ag using SERS, *RSC Adv.*, 2017, **7**, 49969–49974.

36 F. Zapata and C. García-Ruiz, The discrimination of 72 nitrate, chlorate and perchlorate salts using IR and Raman spectroscopy, *Spectrochim. Acta, Part A*, 2018, **189**, 535–542.

37 P. A. Gerakines, W. A. Schutte, J. M. Greenberg and E. F. van Dishoeck, The infrared band strengths of H_2O, CO and CO_2 in laboratory simulations of astrophysical ice mixtures, *Astron. Astrophys.*, 1995, **296**, 810–818.

38 S. Vijayalakshmi and S. Kalyanaraman, Non linear optical analyses of hexamine: phenol cocrystals based on hydrogen bonding: a comparative study, *Spectrochim. Acta, Part A*, 2014, **120**, 14–18.

39 M. Caroff and A. Novikov, LPS Structure, Function, and Heterogeneity, in *Endotoxin Detection and Control in Pharma, Limulus, and Mammalian Systems*, ed. K. Williams, Springer, Cham, 2019.

40 N. Dasgupta and C. Ramalingam, Silver nanoparticle antimicrobial activity explained by membrane rupture and reactive oxygen generation, *Environ. Chem. Lett.*, 2016, **14**, 477–485.